Electrochimica Acta 498 (2024) 144599

Contents lists available at ScienceDirect

Electrochimica Acta

journal homepage: www.journals.elsevier.com/electrochimica-acta

Electrochemical instability of room-temperature ionic liquids with LiTFSI at elevated temperature and its consequences in Li/Li-ion based half-cells and full-cells

Sathish Rajendran, Veka Sri Ganesan, Leela Mohana Reddy Arava *

Wayne State University, Detroit, MI, United States

ARTICLE INFO

Keywords:
Li-ion battery
Room temperature ionic liquids
High-temperature batteries
Cathode electrolyte interphase
Calendar aging

ABSTRACT

High-temperature Li-ion batteries capable of operating up to 100 ℃ can replace lithium thionyl chloride primary batteries in specialized industrial applications. Room-temperature ionic liquids (RTIL) offer high thermal stability and can be a promising choice of electrolyte for high-temperature batteries. This work elucidates that high thermal stability alone does not guarantee effective battery operation due to the electrochemical instability observed in RTIL-LiTFSI mixtures at elevated temperatures. Here, we investigate the impact of varying electrochemical stability in RTILs on half-cell, full-cell, and calendar aging. Electrochemical instability of the electrolyte at the cathode interface injects additional electrons and Li-ions into the electrochemical cell, triggering a cascade of detrimental chain reactions that hinder efficient battery performance. We demonstrate that electrochemical information gathered from a full-cell configuration can frequently obscure the presence of electrochemical instability at the cathode surface. To accurately evaluate this instability, it is essential to perform in-depth half-cell studies and other characterizations. Our results indicate that cathode electrolyte interphase (CEI) can reach a thickness of up to 100 nm, with a depth-dependent composition showing higher concentration of inorganic species like LiF and LiNSO near the cathode surface. Further, accelerated calendar aging measurements of such cells at high temperature revealed complete irreversible self-discharge within as little as 14 days. These findings shed light on the critical factors influencing the stability and performance of cells under challenging operating conditions.

1. Introduction

Li-ion batteries are commonly designed for conventional application within the temperature range of 0 to 45 ℃. Beyond 45 ℃, a thermal cooling system is required to prevent any thermal runway and keep the battery functioning [1,2]. Apart from the conventional applications, there are several applications that demand high energy density Li-ion rechargeable batteries to operate under harsh temperature environments [3]. A major example is the oil and gas industry sector that requires batteries to monitor and power-up sensors during downhole operations at high temperatures. In other industrial applications, safety gadgets such as surveillance cameras, alarms, etc., have to be operated in harsh environments involving high temperature. In another case, in the field of medical industry, the wireless-powered medical devices need to be sterilized periodically at high temperature. Also, military and space applications such as security drones, unmanned aerial vehicles and other high-temperature devices need to be powered by high-temperature batteries. In most cases, a conventional Li-ion battery cannot be used due to the usage of organic carbonate electrolytes that possess low flash points. To meet the diverse demands of high-temperature rechargeable batteries, a significant breakthrough is necessary in current battery materials. Such a breakthrough would enable rechargeable battery chemistry to overcome the predominance of primary Li-ion battery technologies [3]. The current needs for high-temperature batteries are met through lithium thionyl chloride primary batteries that can operate up to 150 ℃ [4]. Replacing primary batteries with rechargeable secondary batteries would reduce the operation cost, maintenance cost, and also promote a clean environment by eliminating the generated battery waste.

Developing Li-ion batteries for high-temperature operation involves many challenges such as developing/identifying thermally stable cathode, anode, separator, electrolyte, and other cell components. Among

* Corresponding author.
E-mail address: leela.arava@wayne.edu (L.M.R. Arava).

https://doi.org/10.1016/j.electacta.2024.144599
Received 30 October 2023; Received in revised form 25 April 2024; Accepted 13 June 2024
Available online 14 June 2024

the various challenges, electrolyte development for high-temperature operation remains elusive due to the thermal instability of the traditionally used carbonate electrolyte solvents. Various strategies have been employed to overcome this limitation by using solid electrolytes, molten-salt electrolytes, and room-temperature ionic liquids (RTILs). Among various options, solid-state electrolyte technology is still underdeveloped and has its own issues and challenges. The molten salt electrolyte is used for very high temperatures, mostly above 200 ℃. At a temperature range of 20 ℃ to 120 ℃, RTILs are a highly viable option due to their high thermal stability. Considerable research efforts in the past have focused on the utilization of various ionic liquids for developing batteries that operate in the temperature range of 40 to 100 ℃ [5–8]. The choice of Li salt in the electrolyte also plays a major role in determining the stability of the electrolyte, particularly with regard to the anion, which determines the nature of interphase formed on the electrodes. $LiPF_6$, a commonly used Li salt, provides unique advantages such as high ionic conductivity and passivation of the aluminum current collector. However, it lacks thermal stability due to the dissociation of $LiPF_6$ into LiF and PF_5 [9]. Salts such as Lithium bis(trifluoromethanesulfonyl)imide (LiTFSI) possess high thermal stability (up to 360 ℃), high chemical stability and low volatility, making them best suitable for high-temperature environments [10–12]. One of the drawbacks of LiTFSI is its ability to corrode the aluminum current collector at about 3.7 V vs. Li/Li^+ that may affect the long-term cycling of the battery [13]. However, LiTFSI will be perfectly suitable for low-voltage cathodes such as $LiFePO_4$ (LFP). LiTFSI in combination with various ionic liquids has been used by other research groups including ours to enable high-temperature operation of Li-ion batteries [14,15]. In several instances, the coulombic efficiency of the battery in the initial cycles has exhibited relatively low. For instance, Kerner et al. developed a polymerized ionic liquid with LiTFSI salt, where the coulombic efficiency at room temperature was measured to be over 94 % in the first cycle with LFP cathode. However, when the temperature was increased to 80 ℃, the coulombic efficiency dropped down to 89 % and then gradually increased to 100 % upon cycling [14]. Nagarajan et al. reported a coulombic efficiency of about 60 % for NMC cathode with phosphonium-based RTIL along with LiTFSI at 100 ℃ without inclusion of any additives [15]. Very little attention has been given to the electrochemical stability of the electrolyte at higher temperature owing to the superior thermal stability of the RTILs and the LiTFSI salt and their wide electrochemical potential window at room temperature. Further, most attention on systems using RTIL electrolytes has been on the anode-electrolyte interphase (SEI) due to the electrochemical reduction of RTILs at the anode surface at lower potentials [16,17].

This study focuses on the electrochemical stability of various RTIL-LiTFSI mixtures at elevated temperature and elucidates their impact on electrochemical cycling. The chemical composition, morphology, and the thickness of the cathode-electrolyte interphase (CEI) formation with the least stable and the most stable RTIL-LiTFSI mixture at elevated temperature has been elucidated using X-Ray photoelectron spectroscopy (XPS) and high resolution-transmission electron microscope (HR-TEM). Additionally, the impact of these CEI characteristics on calendar aging (shelf life) is assessed. The effect of cathodic instability on electrochemical cycling of full cell with a low-voltage cathode (LFP) and high-voltage anode (Lithium titanate, LTO) with different N/P (negative to positive) ratios has been studied in detail.

2. Experimental methods

Electrolyte Stability: Electrochemical stability of the electrolyte at different temperatures was evaluated using linear sweep voltammetry technique. The voltage was swept from the open circuit voltage to 6.5 V vs. Li/Li^+ at a rate of 1 mV/s. Coin cells were fabricated using Li metal (Alfa Aesar) anode and a gold sputtered stainless steel blocking electrode with Celgard PP2075 as the separator. The total electrolyte quantity was 40 μl, 20 μl in each side of the electrode. Various electrolytes were tested by altering the cation of the RTILs. The Li salt and its concentration used was 1 M LiTFSI in the respective RTIL as a solvent. The electrolyte was stirred overnight by a thorough mixing of lithium salt with the RTIL solvent. A hot air oven (MTI Corporation) was used for the measurements at elevated temperature that had a temperature fluctuation of less than 0.1 ℃. In-house customized aluminum cell holders were used for this study. High temperature withstanding wires were used to obtain connection at elevated temperatures.

Cell Fabrication and Testing: Cell fabrication was carried out in an argon-filled glovebox with moisture and oxygen levels less than 0.6 ppm. Half cells in the format of coin cells with lithium metal anode and $LiFePO_4$ (LFP) cathode were fabricated using Celgard PP2075 separator. Coin cells components were purchased from Hohsen and the thermal stability of the components (especially the gasket) was verified to be stable until 110 ℃ before cell testing. The stack pressure inside the coin cell is unknown. 40 μl of electrolytes were added to the cell, 20 μl each side, unless specified. Full cells were made by coupling the LFP cathode and $Li_4Ti_5O_{12}$ (LTO) anode in 14,500 cylindrical cell architecture. 14,500 cylindrical cells (components purchased from MTI corporation) were assembled under standard procedure using LFP and LTO electrode and Celgard PP2075 separator. 750 μl of electrolyte was added to the 14,500 cells in small quantities at fixed time intervals and was held at vacuum (2 min) for the electrolyte to penetrate inside the rolled electrode assembly and the cells were sealed inside the Argon-filled glovebox. The cells were tested at different temperatures mentioned in the results section. LFP electrode composition contained 80 % carbon-coated LFP (MTI corporation), 5 % PVDF binder (Sigma Aldrich), and 15 % C-65 conducting carbon (MTI corporation). LTO electrode composition contained 85 % LTO (MTI corporation), 5 % PVDF, and 10 % C-65 conducting carbon. The theoretical capacity of LFP was considered as 170 mAh/g and LTO as 175 mAh/g for all 'C' rate calculations and cell balancing purposes. The PVDF was dissolved in NMP to make a 10 wt.% solution and then added along with other electrode components and mixed using a vacuum mixer for 90 min along with an appropriate quantity of NMP. The well-mixed slurries were coated onto their respective current collector using the doctor blade technique. The electrode laminates were dried at 80 ℃ and then at 120 ℃ in vacuum for 8 h each to completely dry the NMP. The electrodes were calendared suitably to maintain the electrode porosity around 60 %. The mass loading of the LFP electrodes was about 10 mg/cm^2 (~1.1 mAh/cm^2). The loading of LTO varied according to the N/P ratio mentioned in the results section. All the cells were cycled at C/5 rate unless specified. Linear sweep voltammetry, chronoamperometry, and electrochemical impedance spectroscopy were performed using a Biologic SP300 bipotentiostat. Cycling of half-cells and full-cells in coin cell format was performed using an Arbin cycler. The testing of cylindrical cells was carried out using a Landt cycler.

Characterization Techniques: High-resolution transmission electron microscope (HRTEM) images of the cycled electrodes were obtained using Talos F200X G2 instrument. The cycled electrodes were obtained by decrimping the cycled cell in a glovebox. The obtained electrode was rinsed using dimethyl carbonate (DMC) solvent to remove any residual electrolyte salt and dried in vacuum for 2 h. A small quantity of electrode material was scraped from the current collector and added to a glass vial with DMC solvent. The electrode material agglomerated was dispersed in the DMC by ultra-sonicating it for 30 min. The dispersed material was pipetted onto a lacey carbon-coated copper TEM grid (Ted Pella) inside the glovebox. The TEM grid was transported from the glovebox to the instrumentation center in an air-tight Mason jar and transferred to the instrument with minimal ambient exposure. The X-ray photoelectron spectroscopy (XPS) was performed on the rinsed electrode directly using a Nexsa G2 surface analysis system. The sample was transferred to the instrument using a vacuum transfer module. The XPS samples had zero exposure to the ambient atmosphere. All the H^1, C^{13}, F^{19}, and Li^7 NMR experiments were carried out in a Varian 600 MHz NMR spectrometer. There were two types of NMR samples for analysis: fresh and cycled

electrolytes. The separators from the cycled cells containing 1 M of LiTFSI in Py RTIL were removed from the decrimped coin cells and washed in the deuterated solvent, dimethylsulfoxide-d_6 (d-DMSO; Sigma Aldrich), in a vial. The fresh electrolytes were diluted in d-DMSO in the ratio 1:10 respectively. 0.7 ml of each solution (fresh and cycled samples) was pipetted into an NMR tube and sealed inside the glove box using a polyethylene cap.

3. Results and discussion

3.1. Electrochemical Stability of RTILs with LiTFSI at higher voltages

RTILs are made up of a bulky organic cation and an inorganic anion that exists in the liquid state at room temperature. Properties of the RTILs such as electrochemical stability, chemical stability, viscosity, density, and conductivity are greatly dependent on the nature of the cation and anion. Among various choices of anions, the anion used in this study was fixed as $TFSI^-$ due to its ease of synthesis and relatively high electrochemical, chemical, and thermal stability [18]. Different cations were explored, such as pyrrolidinium (Py), piperidinium (Pip), ammonium (Am), imidazolium (Im), and phosphonium (Ph). The electrochemical stability of the electrolytes with 1 M LiTFSI salt was evaluated using linear sweep voltammetry (LSV). The potential was swept from the open circuit voltage to 6.5 V with a gold-coated stainless steel blocking electrode as cathode and Li anode. The LSV tests were performed at three different temperatures, 22 ± 1 ℃ (room temperature), 60 ℃, and 100 ℃, for each ionic liquid, as shown in Fig. 1. Any electrochemical instability in the electrolyte will be indicated by an increase in current during voltage sweeping towards higher potentials. In the zoomed-out regions of Fig. 1, all five electrolytes appeared to exhibit very high electrochemical stability until 5 V at all three temperatures. However, the zoomed-in inset shows a different story. All electrolytes exhibited superior stability until at least 4.2 V at room temperature. Above 4.2 V, the increase in current is very insignificant until about 5–5.2 V after which the current drastically increases indicating rapid oxidation of electrolyte at the electrode. Most commercial cathodes operate under 5 V. and hence, the electrochemical instability of the electrolytes above 5 V should not be of any problem and the obtained values are much higher than the stability of conventional organic, carbonate-based electrolyte systems. When the temperature is increased to 60 ℃, there is an existence of an additional shoulder peak above 3.4 V for electrolytes with Py, Pip, Im, and Am (Fig. 1a–d), which indicates the oxidation of anions present in the electrolyte ($TFSI^-$) over the cathode surface. The presence of shoulder peak only at 60 ℃ and not at room temperature indicates that the electrochemical instability is triggered by the increase in temperature. Ph RTIL did not exhibit any significant shoulder peak at 60℃ (Fig. 1e); however, the major oxidation shifts to the lower potentials similar to other RTILs. At 100 ℃, the intensity of the shoulder peak increased drastically indicating accelerated oxidation for Py and Am RTILs (Figs. 1a, d, S1) and the peak position further shifted to the lower potentials for most of the RTILs. A comparison plot of the various RTILs at 100 ℃ is shown in Fig. S1. Ph RTIL exhibited an increase in current above 3 V indicating parasitic reactions at the cathode surface; however, the increase in current is relatively low when compared to the instabilities of other RTILs at 100 ℃.

At elevated temperatures, the Py and Am RTILs exhibited poor stability, while the Ph RTIL exhibited relatively higher stability. This trend in electrochemical stability with a variation of cations is in alignment with the results observed by Rogers et al. using mercury electrodes at room temperature [18]. The change in electrochemical stability with different RTILs is related to the change in solvation and ion-pairing effects of $TFSI^-$ anion with various cations [19]. Association of electrochemical stability of the electrolyte to the HOMO-LUMO or the oxidation/reduction potential is a debated topic and for this current study, we will stick with the latter [20]. The oxidation potential of the electrolyte (E_{OX}) tends to reduce with the increase in temperature, as represented in Fig. 1f. Overall, the thermally stable RTIL-based electrolytes exhibit electrochemical instabilities at higher temperatures above 3 V vs. Li/Li^+. The instabilities depend on the type of cation and anion of the RTIL being used.

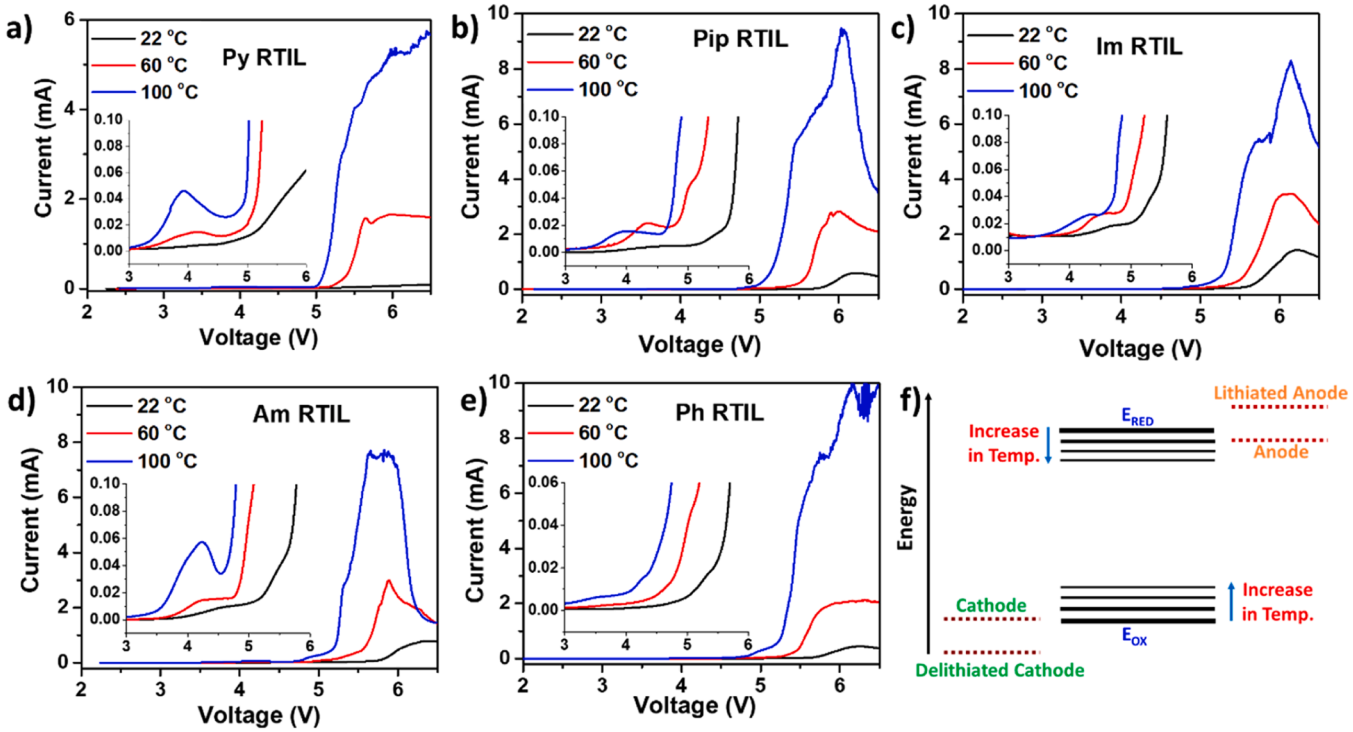

Fig. 1. Electrochemical stability measurement at different temperatures using linear sweep voltammetry for RTILs with a) Pyrrolidinium, b) Piperidinium, c) Imidazolium, d) Ammonium, and e) Phosphonium cations. e) Schematic representation of the variation in oxidation potential of electrolyte with temperature and its difference with the energy levels of the cathode.

3.2. Effect of electrochemical instability of RTILs on half-cells

The effect of poor electrochemical stability of the RTIL-based electrolytes at elevated temperature on electrochemical cell performance was demonstrated by testing the electrolyte in half-cells using a low voltage cathode, $LiFePO_4$ (LFP), and Li metal anode at 100 ℃, as shown in Fig. 2. Three different electrolytes with various cations were chosen from the pool of electrolytes. The choice of cation was determined based on testing an electrolyte with relatively very low electrochemical stability (Py), intermediate stability (Pip), and high stability (Ph). The specific discharge capacity varied drastically during electrochemical cycling for all three electrolytes (Fig. 2a). The cells with Py and Ph RTIL exhibited similar discharge capacity (~140 mAh/g) during the initial cycles and the capacity was lower (~122 mAh/g) for the cell with Pip RTIL. The specific capacity of Py RTIL dropped drastically during cycling, resulting in a 57 % capacity retention after 50 cycles. The capacity fade in cells with Ph RTIL was very minimal (~95 % capacity retention in 45 cycles) and exhibited perfect cycling when compared to the other electrolytes. The cell with Pip RTIL demonstrated increasing capacity in the initial 10 cycles after which the capacity stabilized during the subsequent cycles. The specific capacity of the cell with Pip RTIL was higher than the Ph RTIL cell during the prolonged cycling, which could be from the difference in viscosity between the electrolytes. The viscosity of Pip RTIL is much lower than Ph RTIL that may enable better wetting of the cathode surface.

The trend in coulombic efficiency (Fig. 2b) was similar to the specific capacity; the cell with Ph RTIL recorded the highest value followed by Pip and Py RTILs. The average coulombic efficiency was 99.01, 97.16, and 94.47% for the cells with Ph, Pip, and Py RTILs, respectively. The 1st cycle efficiency was only 65%, and 75% for the Py and Pip RTIL, respectively, which is very low to achieve any full-cell performance. The corresponding voltage profiles of the cells are shown in Fig. 2c–e. The cell with Py RTIL exhibits very unusual behavior during the charging of the cell (Fig. 2c). The charging capacity of the 1st cycle is about 210 mAh/g, which is higher than the theoretical capacity of LFP (170 mAh/g). The discharge capacity curve exhibits a typical LFP behavior as observed with the conventional electrolyte at room temperature [21]. The unusually high capacity during the first cycle eventually reduces during the subsequent cycles along with a drastic fade in cell capacity. A cell with Py RTIL was just charged once at 100 ℃ and later decrimped to check for any changes in the electrode and electrolyte, as shown in Fig. S2. The electrolyte turned from a colorless liquid to a reddish-brown colored liquid indicating severe decomposition of the electrolyte in just one charging reaction. To validate any iron dissolution from LFP, the energy-dispersive X-ray (EDX) spectra (Fig. S3) were recorded for the cycled separator, and it did not indicate any iron (Fe) peak over the separator surface. The same electrolyte was also used with NMC 111 cathode with the same cut-off used for the LFP cell and the decrimped cell after cycling looked identical along with poor coulombic efficiency values, as shown in Fig. S4. This confirms that the decomposition is because of the electrolyte and not any metal dissolution. The Pip RTIL cell exhibited a charge capacity of 165 mAh/g and a discharge capacity of 123 mAh/g in the first cycle. Although the charge capacity is not as high as in the case of Py RTIL, the difference between the charge and discharge capacity indicates that significant irreversible reactions occur in the cell. The subsequent cycles resulted in a decrease in charge capacity and an increase in the discharge capacity. The cell with Ph RTIL exhibited a charge and discharge capacity of 152 and 136 mAh/g, and the variation in capacities after the first cycle is relatively less compared to the other cells. A comparison plot of the 1st voltage profile of the three different RTILs at 100 ℃ is shown in Fig. S5, which depicts the trend in the first charge capacity of the three different RTILs used.

A clear relationship between the cell performance, especially the charge capacity, and the electrochemical stability of the electrolyte exists at elevated temperatures. The unusually high capacity observed with electrochemical instability of the electrolyte arises from the parasitic current produced from the decomposition of the electrolyte. The anion species in the electrolyte, $TFSI^-$, oxidizes over the cathode, resulting in the injection of electrons to the cathode, which along with the electrons from the active material moves to the anode. The electrons in the anode combine with Li^+ present in the electrolyte resulting in the plating of Li over the surface of the Li metal. Hence, there are two sources of

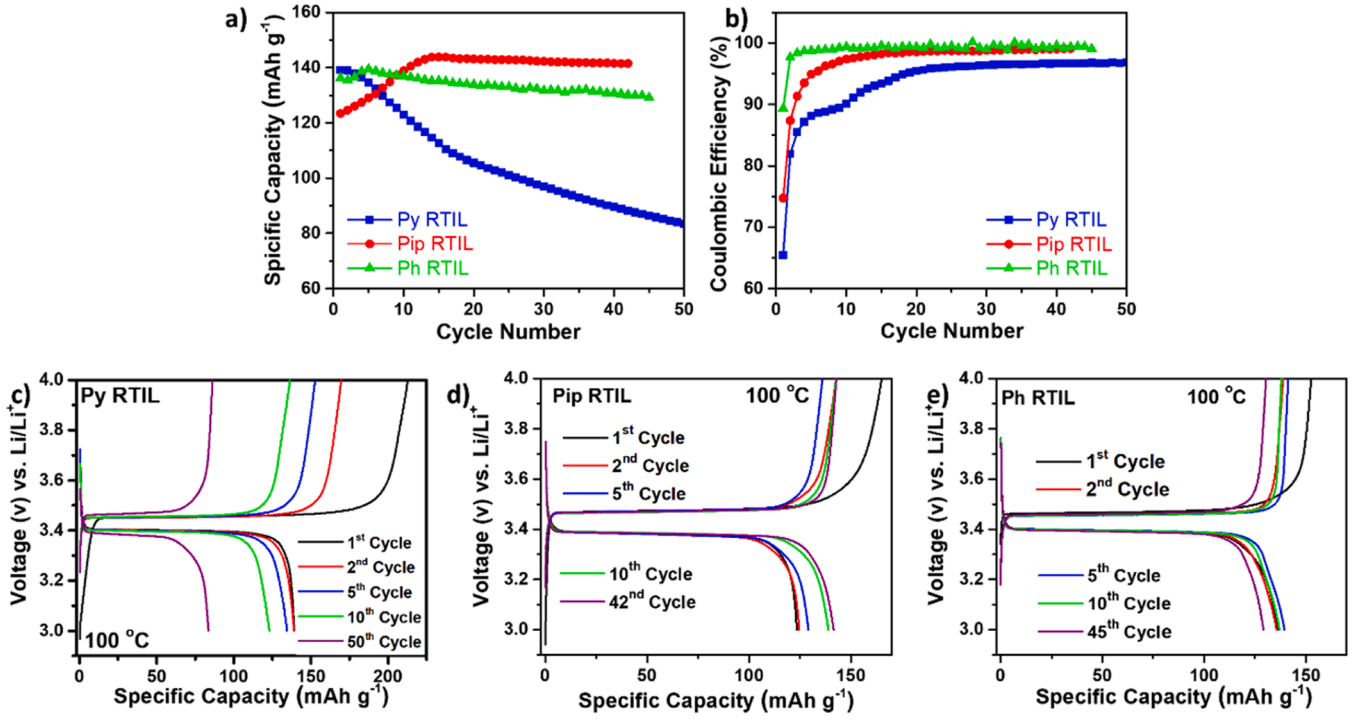

Fig. 2. a) Specific capacity and b) Coulombic efficiency chart obtained from the electrochemical cycling of a half-cell with LFP cathode at 100 ℃ and their corresponding voltage profile with c) Pyrrolidinium, d) Piperidinium, and e) Phosphonium cation containing RTILs.

electrons, one from the redox of the cathode active material and the other from the oxidation of anion species of electrolyte. Electrons from both sources end up getting consumed during the Li plating step. If the stated hypothesis is correct, there should be two phenomena that must take place.

I. The unusual capacity must vary with the electrolyte quantity.
II. The concentration of LiTFSI must decrease in the electrolyte due to the oxidation of $TFSI^-$ on the cathode and the subsequent reduction of Li^+ on the anode.

Now to the validation of the hypothesis following experiments have been performed.

3.3. Relationship between charging capacity and electrolyte quantity

The variation of electrochemical performance of half-cells with the quantity of electrolyte was investigated by testing half-cells with three different electrolyte quantities, 6, 12, and 20 μL with the least stable electrolyte, Py RTIL, at 100 ℃, as shown in Fig. 3. 6, 12, and 20 μL electrolyte quantities refer to the electrolyte added in the cathode side and the same quantity of electrolyte is also added in the anode side. As evident from the specific capacity chart in Fig. 3a, the half-cell performance is correlated with the quantity of electrolyte present. The cell with 6 μL exhibited a low initial capacity, 123 mAh/g, and it increased further to exhibit a relatively stable performance. The cell with 12 μL electrolyte exhibited a higher capacity of 135 mAh/g, but the performance gradually faded in the subsequent cycles. Although the cell with 20 μL exhibited the highest first-cycle capacity, the capacity drastically faded upon cycling. The variation in the first cycle capacity is probably due to the improved wetting of the cathode with the electrolyte. However, the capacity fade is determined by the quantity of electrolyte in the cell that may promote the delamination of the electrode during the electrolyte oxidation on the cathode. The variation of coulombic efficiency with electrolyte quantity (Fig. 3b) depicts a clear trend in the efficiencies obtained with various quantities of electrolytes. The efficiency was found to be inversely proportional to the quantity of electrolyte in the cell. The cell with a higher quantity of electrolyte exhibited a lower efficiency, which clearly indicates a higher amount of electrolyte oxidation with higher quantities of electrolyte. The corresponding voltage profiles of the first three cycles of the half-cells are shown in Fig. 3c–e. There is a clear variation of the first cycle charge capacity with the increase in electrolyte quantity. The cell with 6 μL electrolyte exhibited comparatively higher polarization because of the improper wetting of the cathode due to the insufficient electrolyte. On the other hand, the efficiency seemed to be much better than the other cells. The results obtained seemed to support the hypothesis of $TFSI^-$ oxidation over the cathode surface.

3.4. LiTFSI Concentration variation with electrochemical cycling

To probe the changes in LiTFSI concentration during electrochemical cycling, *ex-situ* NMR spectroscopic analysis on the fresh and cycled electrolyte was carried out. It is known that in Py RTIL containing LiTFSI, there is a formation of a solvated complex, $[Li(TFSI)_n]^{(n-1)-}$. Depending on the concentration of $TFSI^-$anions, the number of $TFSI^-$ ions coordinated to Li^+ varies, and usually more than one $TFSI^-$ anions are coordinated to Li^+ in the first solvation shell, and there is a continuous exchange between the anions of the first solvation shell with the later. For 1 M of LiTFSI in Py RTIL, the solvated complex or the adduct, $[Li(TFSI)_2]^-$ is usually formed [22]. The extent of interaction of the cation with the anion depends on the size of the cation, and Py cation, being large, interacts only to a little extent with $TFSI^-$ anion [23]. The H^1 NMR plots of fresh electrolyte, once-charged electrolyte, and cycled (10 cycles) electrolyte are shown in Fig. 4a. The different protons in the Py cation are marked in the chemical structure (Fig. S6) given and indicated in the NMR plot (Fig. 4a). The H^1 NMRs of fresh electrolyte and cycled electrolyte were compared, and no major changes in the peaks were noticed between the two, which means no new bond formation occurred. This shows that there are no decomposition

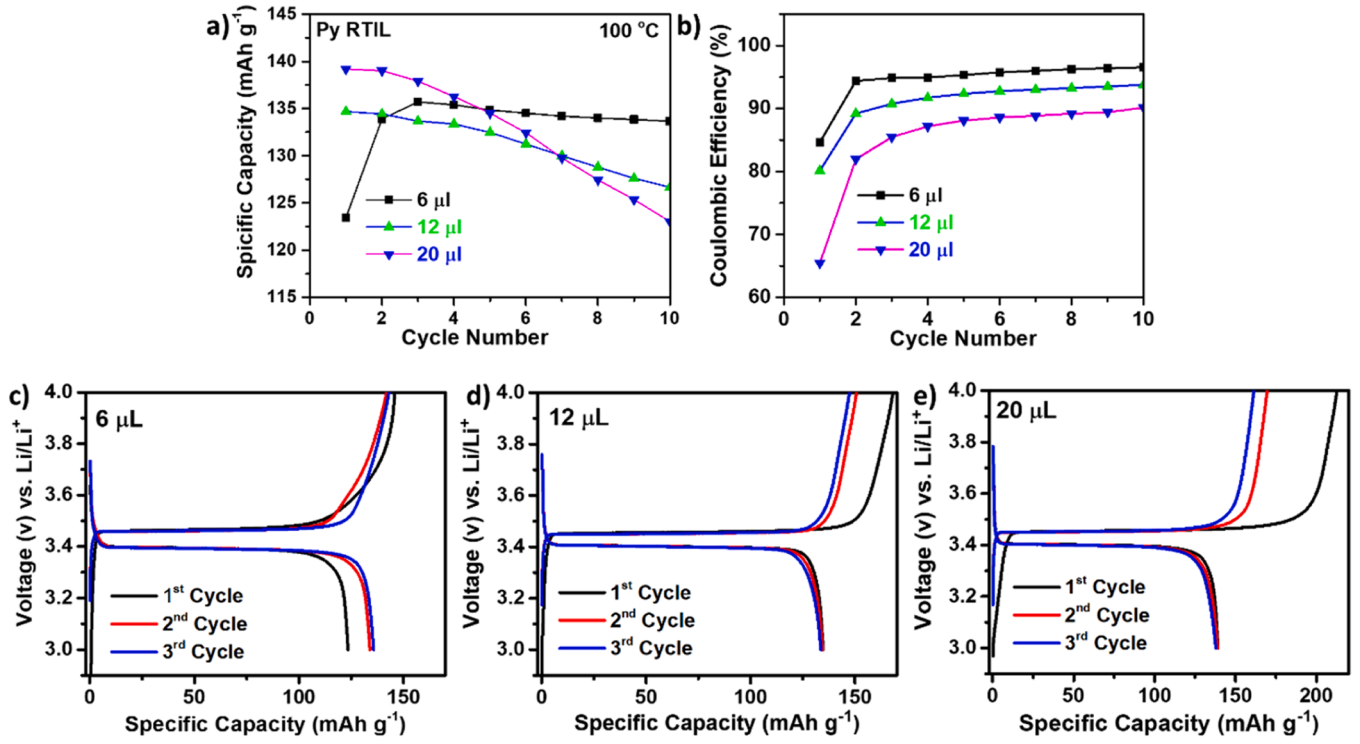

Fig. 3. a) Specific capacity and b) Coulombic efficiency chart obtained from the electrochemical cycling of a half-cell with LFP cathode at 100 ℃ by varying the quantity of Py RTIL electrolyte and their corresponding voltage profile with c) 6 μL, d) 12 μL, and e) 20 μL.

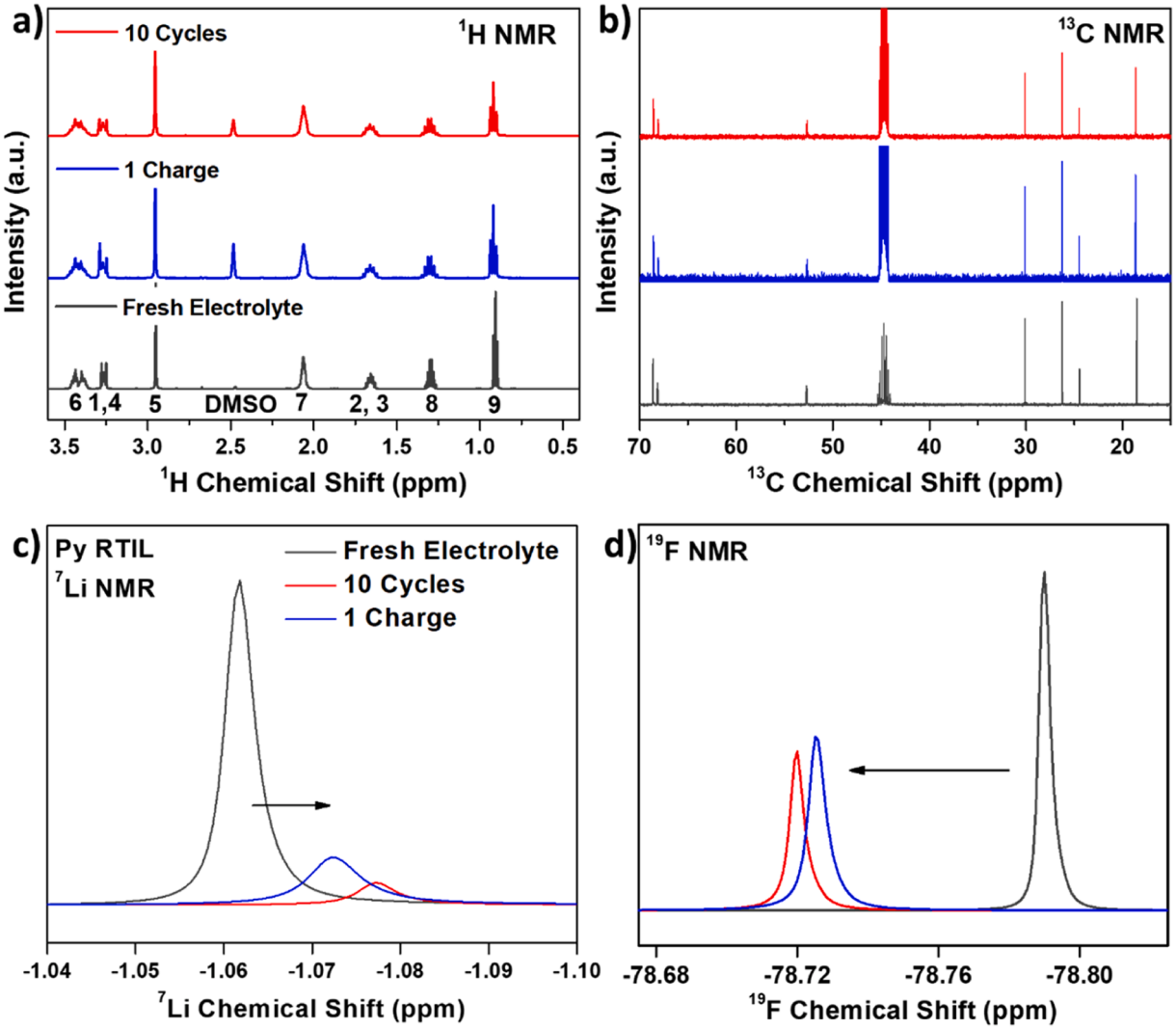

Fig. 4. a) ^{1}H, b) ^{13}C, c) ^{7}Li, and d) ^{19}F NMR spectra of the fresh and cycled electrolyte using half-cell with Py RTIL at 100 °C.

products in the electrolyte after cycling. In literature, no variations have been noted previously between the H^1 NMRs of pure Py RTIL and LiTFSI doped Py RTIL but there exists a coulombic interaction between the $TFSI^-$ ions and the hydrogens in the ring and -CH_3 of both methyl and butyl groups (marked as 1, 2, 3, 4, 5 and 9 in the structure) in both the samples [24]. This indicates that irrespective of the concentration of LiTFSI in the RTIL, there is always a dipolar interaction between the $TFSI^-$ ions and Py cations. Hence, it is right to assume that the same interaction exists in the electrolyte samples we have considered.

Fig. 4b shows the C^{13} NMR of the fresh and cycled electrolyte. The coulombic interaction mentioned above not only influences the hydrogens, but also the carbons marked 1, 2, 3, 4, 5, and 9. However, no major peak shifts occur owing to the interaction being only electrostatic. The -CF_3 (from $TFSI^-$) quartet peaks (around 120 ppm) for the cycled electrolyte have narrowed in comparison with the fresh electrolyte. This shows that the -CF_3 groups in the cycled electrolyte have a more symmetrical electron density around them than those of the fresh electrolyte. This could chiefly be due to the changes in the solvation structure and the Li^+-$TFSI^-$ aggregates that exist in the electrolyte. This change can be brought about by the concentration variations of a particular solvation species that occur with cycling.

In Fig. 4c, changes can be observed in the Li^7 NMR where the peak shifts from −1.06 ppm to −1.08 ppm for the cycled electrolyte. There also exists a coulombic interaction between Li^+cation and Py cation through the TFSI- anion interacting electrostatically with both the cationic species. A minor shift of 0.01 ppm (chemical shift to −1.072) was observed even for the electrolyte with just one charge. The minor shift in the Li^7 NMR has been similarly observed for variation in LiTFSI concentration before [25]. With a decrease in the LiTFSI concentration, the number of solvated species forming aggregates must have lowered with a lesser number of $TFSI^-$ anions interacting with Li^+ after cycling. The decreased number of $TFSI^-$ anions coordinated to Li^+ results in Li^+ being more shielded than it was before cycling. We can also corroborate that since Py^+ interacts with Li^+ through $TFSI^-$, the interaction between both the cations decreases as the $TFSI^-$ anions gradually decrease from the electrolyte with cycling.

The F^{19} NMR peak of the fresh electrolyte shifts from −78.79 ppm to −78.72 ppm for the cycled electrolyte as shown in Fig. 4d, which indicates that the F in $TFSI^-$ moves from a more shielded environment to a slightly less shielded environment on cycling. The fluorine in $TFSI^-$ is involved in the dipolar interaction that is present between $TFSI^-$ and Py^+ that was mentioned in the H^1 NMR section [26]. The F^{19} chemical shift can be associated with the changes observed in the C^{13} NMR for the -CF_3 group in $TFSI^-$. The downfield shift indicates decreased coulombic interaction of the F in the $TFSI^-$ species with the other electrolyte species. Nicotera et al. show in their experiments that the F^{19} NMR peak shifts downfield when the concentration of LiTFSI is lowered in the RTIL-based electrolyte and state that, increasing the LiTFSI

concentration results in the interaction between $TFSI^-$ and Li^+ [25]. Similar to Li^7 NMR spectra, a shift from −78.79 ppm to −78.73 was observed with the sample which was charged once, indicating the rapid decrease in concentration of TFSI- ions in a single charge. Therefore, compared to the fresh electrolyte, the Li^+-$TFSI^-$ interaction in the cycled electrolyte has decreased, which indicates that the concentration of $TFSI^-$ in the electrolyte has reduced with cycling.

Based on solid evidence of the electrolyte instability mechanism in half-cells, further investigations are undertaken to understand the impact of the electrolyte instability on full-cell performance.

3.5. Effect of electrochemical instability of RTILs on full-cells

Full-cells in the format of 14,500 cylindrical cells with LFP cathode and LTO anode were fabricated and tested using standard procedure. Py RTIL was used as the electrolyte and the testing temperature was 100 ℃. Conventional anode, Graphite, was not used here because of the preferential RTIL cation intercalation into graphite resulting in the exfoliation of graphitic sheets from the electrode [27]. A standard N/P (areal capacity of negative to positive electrode) ratio used in conventional Li-ion batteries, 1.05, was used to fabricate these cells [28]. The electrochemical performance, as shown in Fig. 5a, appeared to show a typical Li-ion battery performance. The first cycle (formation) charge and discharge capacity of the cell were 254 and 210 mAh, respectively that account for an efficiency of about 85 %. The subsequent cycles exhibited uniform performance with a discharge and charge capacity of about 207 mAh with an efficiency of over 99.5 %. The presence of any electrochemical instability did not seem to exist according to the electrochemical performance of the full-cell.

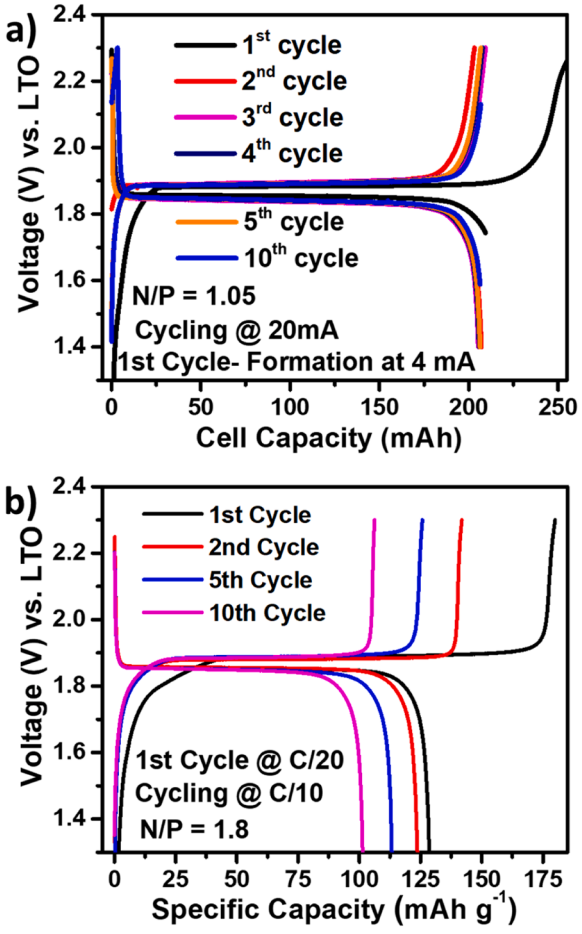

Fig. 5. Voltage profile of the full-cell during electrochemical cycling with LFP cathode, LTO anode and Py RTIL at 100 ℃ with the N/P ratio of a) 1.05, and b) 1.8.

One possible hypothesis is that despite the cell exhibiting perfect electrochemical performance, there is a likelihood for the masking of electrochemical instability taking place in the cathode of a full cell at elevated temperature. The electrolyte being oxidized in the cathode injects additional electrons that move to the anode via the external circuit. Once the electron reaches the anode, it ends up reducing the Li^+ in the electrolyte over the Li metal anode surface in a half-cell. In full-cells with LTO anode, the Li^+ present in the electrolyte will result in intercalating with the anode. But the key point here is that LTO can only accept Li^+ until its theoretical capacity is reached. Here, the theoretical areal capacity of LTO is just 5 % higher than the theoretical areal capacity of the LFP used. Hence, the LTO accepting the electron and Li^+ is limited in the case of full-cell, and Li metal has unlimited ability to accommodate Li^+ and electrons as it is the plating reaction that occurs over the Li anode in the case of half-cells. Although the electrolyte may be oxidizing over the cathode in full-cells, the LTO does not have the capacity to accept both the electrons originating from the cathode active material and the parasitic (oxidization) reaction over the cathode surface. If the electrolyte oxidation occurs over the cathode surface, there is a high probability that LFP is not completely delithiated. At the end of a charging step, the cell will polarize depending on the anode potential and not the cathode potential resulting in an underutilized LFP in the cell. Validating the above-mentioned hypothesis, the best method is to test a cell with a high N/P ratio that would enable LTO to accept a higher number of electrons and Li^+ than the one coming from the LFP cathode.

Fig. 5b shows the voltage profile during electrochemical testing of a full-cell at 100 ℃ in a coin cell format with a high N/P ratio with the same Py RTIL electrolyte. As evident from the figure, the electrochemical performance of the cell varies drastically depending on the N/P ratio. The first charge capacity was about 180 mAh/g, which is higher than the theoretical capacity of LFP cathode used. The first discharge efficiency was about 128 mAh/g, with an efficiency of just 71 %. The capacity decays faster during the subsequent cycles, that is completely contrary to what was observed in a cell with a low N/P ratio. This indicates that electrolyte oxidation occurs over the surface of the cathode irrespective of the cell's anode material. However, the important point to keep in mind is that the parasitic reactions occurring at the cathode in a full cell will be masked if the N/P ratio is close to or less than 1. Moreover, the prolonged cycling of the cell will consume the electrolyte and result in poor cycle life of the battery, along with additional issues like high amount of gassing which plays a critical role in the safety of the battery at elevated temperatures. Despite the gassing issue, the cells will not impose a fire hazard because of the use of RTIL electrolyte. In the subsequent sections, the reaction products of the RTIL-LiTFSI oxidation over the cathode surface will be elucidated using advanced characterizations.

3.6. Stability of the cathode electrolyte interphase (CEI) with RTIL at elevated temperature

The NMR results shown in Fig. 4 are clear evidence that there are no additional reaction products present in the electrolyte of the cycled battery. There are two possibilities about what reaction products form during the electrolyte oxidation and where: (i) over the cathode surface to form a cathode electrolyte interphase (CEI), (ii) electrolyte oxidation leading to gas formation, or both. To investigate the above-mentioned issues two characterization techniques, high-resolution transmission electron microscopy (HR-TEM) and X-ray photoelectron spectroscopy (XPS), have been used to probe the morphology and chemical constituents of the cathode surface, as shown in Fig. 6. Two different electrolytes were investigated, the least stable Py RTIL and the relatively stable Ph RTIL, with LFP cathode at 100 ℃. The selected particles were confirmed to be cycled LFP using EDX spectra, as shown in Fig. S7.

The HR-TEM images of a cycled LFP particle using Py RTIL are shown in Fig. 6a, b. A thick layer of CEI can be found over the LFP particle. The

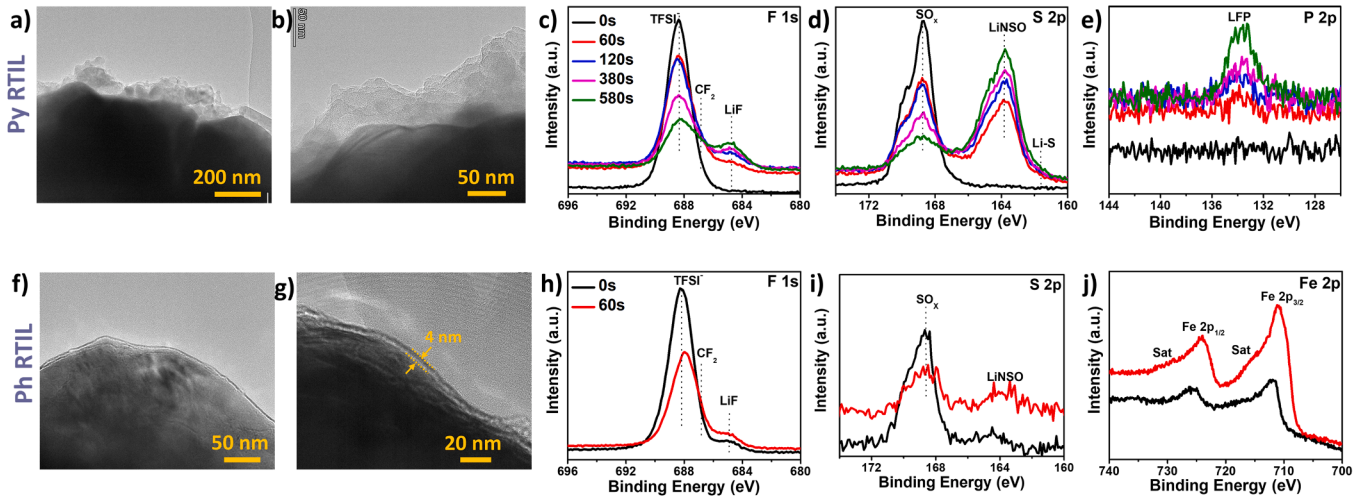

Fig. 6. Characterization of the cathode electrolyte interphase formed over the cycled LFP particles using a–e) Py RTIL and f–j) Ph RTIL at 100 ℃. a, b, f, g) HR-TEM of the LFP cathode particle, and c–e, h–j) X-Ray photoelectron spectra investigation of the CEI composition using depth profiling of the cathode surface.

thickness of the CEI was not uniform and was found to vary from 25 nm to over 100 nm. The thickness of the CEI was very high when compared to a few nanometers in conventional Li-ion batteries at room temperature [29,30]. The composition of the CEI has been elucidated using XPS (Fig. 6c–e). As the inelastic mean free path of the X-ray used is less than 5 nm for such materials, depth profiling was carried out using Ar^+ to probe any changes in composition with the depth of the CEI [31]. The F 1 s spectra (Fig. 6c) on the top surface (0 s) exhibit one single peak at 688.4 eV that corresponds to the fluorine present in the $TFSI^-$ anion [32]. Upon etching the surface, there is an additional shoulder peak at 684.8 eV that corresponds to LiF [33]. LiF is an important CEI constituent that is known for its role in stabilizing the CEI in a conventional Li-ion battery [34]. The LiF peak increases upon etching the surface, indicating that the concentration of LiF increases upon the depth of the CEI. Despite the presence of LiF toward the LFP particle, it failed to stabilize the CEI at elevated temperatures. Upon prolonged etching beyond 120 s, there is an additional shoulder peak at 686.8 eV corresponding to the CF_2 peak from the PVDF binder [35]. The S 2p spectra (Fig. 6d) at the top surface show two sets of doublet peaks corresponding to SO_x at 167. 2 and 168.8 eV (Fig. S8a) [32]. Upon etching, there is an increase in another major set of doublet peaks at 163.8 eV (Fig. 6d). The literature identifies this peak to be LiNSO, a decomposition product of similar ionic liquid in the CEI [33,36] Deconvolution of this peak (Fig. S8b) shows an additional doublet at 161. 8 eV corresponding to Li-S bond containing species, most likely Li_2S [21]. The SO_x peak drastically decreases in intensity followed by an increase in intensity of the LiNSO peak during etching. To ensure this is not from the beam damage of the X-rays, Ar^+ etching of LiTFSI salt was carried and the LiNSO peak was not found in the S 2p spectra, as shown in Fig. S9. The P 2p spectra (Fig. 6e) did not show any signal on the top surface, which could be due to the thick CEI that is being formed on the surface. However, the P 2p peak of LFP slowly arises upon etching. This confirms that the CEI is highly thick over the LFP electrode cycled at elevated temperature using Py RTIL and the composition of the CEI is dependent on its depth. The top surface is mostly the residual LiTFSI salt and upon depth, the decomposition products of the $TFSI^-$ oxidation could be probed.

The HRTEM image of the LFP particle cycled using Ph RTIL at 100 ℃ is shown in Fig. 6f, g. The image shows an ultra-thin conformal CEI layer above the LFP particle, with a thickness of about 4 nm. The F 1 s spectra (Fig. 6h) show two distinct peaks of $TFSI^-$ and LiF on the surface. Upon etching for 60 s, the $TFSI^-$ peak decreases and LiF peak increases, similar to Py RTIL. This indicates that the CEI is indeed depth-dependent in the case of Ph RTIL; however, the thickness of the CEI is much smaller than the Py RTIL. The S 2p spectra (Fig. 6i) show one set of doublets with very low intensity corresponding to the SO_x and a very small shoulder corresponding to the LiNSO that does not increase drastically upon etching, unlike Py RTIL. The Fe 2p spectra (Fig. 6j) indicate that the CEI thickness is not more than the inelastic mean free path of the CEI, about 4–5 nm. Here, P 2p was not used as a reference because of the presence of phosphorus in the ionic liquid, which is not the case with Py RTIL. The major difference between the CEI of the cell cycled using Py RTIL and Ph RTIL is the thickness and the presence of a larger quantity of LiNSO, which is a decomposition product of the LiTFSI salt. The CEI formed using Ph RTIL was able to passivate the cathode surface from subsequent decomposition of electrolyte, whereas the Py RTIL CEI was not able to protect the LFP cathode.

The quantification of the atomic composition from the EDX spectra of the cycled cathode with Py RTIL and Ph RTIL electrolytes was tabulated in Table S1. For the cathode cycled with Py RTIL, it was noted that the ratio of Fe:P:O was 1.12:1:2.54, which does not match the formula of LFP ($LiFePO_4$). However, for the cathode cycled with Ph RTIL, it was found that the ratio of Fe:P:O was 0.92:1:4.68 from the quantification table. This closely matched the formula of LFP suggesting that compared to Py RTIL, the LFP particles in the cathode cycled with Ph RTIL were more stable after cycling. The ratios of C:N:F:S in the cathodes cycled with Ph RTIL and Py RTIL were calculated to be 22.25:0.19:1:0.02 and 10:0.34:1:0.023, respectively. The higher ratio of C in the Ph RTIL could suggest that the decomposition products on the CEI could be majorly from the contribution of the organic cation of the RTIL. However, in the cathode cycled with Py RTIL, a slightly higher ratio of N and S was noted, which could be the result of TFSI decomposition.

3.7. *Calendar Aging of high-temperature batteries*

In the previous sections, the effect of the electrochemical instability of the RTIL-LiTFSI mixture on half-cells and full-cells has been elucidated. The full-cells with an N/P ratio close to 'one' did not exhibit any capacity fade or abnormal behavior during the electrochemical cycling because of the higher electron and Li^+ inventory cycling within the cell. In this section, an additional phenomenon that affects such cells during their storage at a partially/fully charged state is discussed in detail. The calendar life/ shelf life of a cell refers to the amount of time that it can be stored without any irreversible changes occurring resulting in permanent capacity loss. The reactions and their outcome in a cell during calendaring aging are shown in Fig. 7a. When the cell is fully charged or partially charged, the cathode will experience a higher potential than the ground state. The higher potential that the electrode experiences may induce an oxidation reaction to occur over the cathode surface

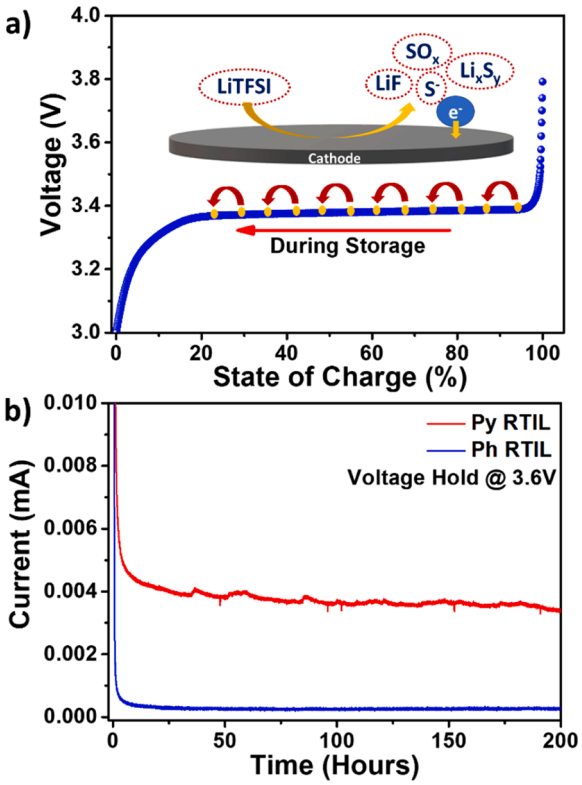

Fig. 7. a) Mechanism of self-discharge during calendar aging, and b) accelerated calendar aging test using chronoamperometry.

when the cell is stored after the charging process. The anion of the electrolyte oxidizes over the cathode surface, and the resulting electrons will travel to the anode only if the external circuit is complete, as in the case of charge/discharge. When the cell is being stored, the external circuit is 'open' that prevents the electrons from moving to the anode. This results in the cathode accepting the electrons and Li^+ from the electrolyte decomposition and thus the cathode gets lithiated irrespective of any reaction on the anode side. The state of charge of the cell decreases as the cathode is lithiated and the electrolyte is consumed in the cell during this process. Further, the anode will be in the lithiated state when fully charged, and the cathode gets lithiated during self-discharge occurring during storage resulting in drastic permanent capacity loss in cells.

Calendar life predictions can be extremely time-consuming as the calendar life of conventional batteries at room temperature can be anywhere in between five to twenty years [37]. This period can be relatively less for high-temperature batteries using RTIL electrolyte due to the higher rate of parasitic reactions. However, estimating the calendar life is still a time-consuming process. A chronoamperometry-based technique has been used to evaluate the calendar life of cells at elevated temperature, as shown in Fig. 7b. A half-cell with LFP cathode and two different electrolytes, Py and Ph RTIL, is held at a potential slightly above the fully charged state and the steady-state current is used to evaluate the calendar life by correlating it to the 'C' rate of the cell. Ideally, the current should be infinitesimally small because the cell electrode will polarize when applied with a higher potential above the fully charged state of the electrode and the resulting current will be from the parasitic reaction, if any. The steady-state current from the cell with Py RTIL was about 3.6 μA and Ph RTIL was about 0.313 μA, which correspond to a calendar life of 302 h (~13 days) and 3476 h (~145 days), respectively. This indicated that the cathode will be completely lithiated in 13 days in the cell with Py RTIL and 145 days in the cell with Ph RTIL at 100 °C. However, this method assumes that the cell is in the fully charged state for the entire process. In practical conditions, the electrolyte reactivity decreases as the state of charge of the cathode lowers and also the voltage is held at a slightly higher potential than the actual cathode potential when fully charged. Hence, the actual calendar life will be slightly higher than the one predicted using this method. However, the rough estimates of 13 days and 145 days are very much lower to achieve any practical cell at elevated temperature using the mentioned ionic liquids. Further, this method is more accurate for cells with flat voltage profiles as the extent of cathode reactivity at different states of charge is almost the same.

4. Conclusion

Despite room-temperature ionic liquids (RTILs) possessing high thermal stability up to 300 °C, the electrochemical stability needs in-depth investigation before employing them in high-temperature batteries. The electrochemical stability of various RTILs with LiTFSI salt at elevated temperature has been investigated and is found to strongly depend on the type of cation used in the RTIL. Pyrrolidinium and Ammonium based RTILs exhibit the least stability and Phosphonium based RTILs demonstrate the highest stability. The electrochemical instability of RTILs directly affects the half-cell performance resulting in an unusual excessive charge capacity and drastic capacity fade. The anion present in the electrolyte oxidizes over the cathode surface resulting in additional electrons traveling to the anode, where additional Li-ions from the electrolyte reduce over the anode surface. The excessive charge capacity was found to be dependent on the electrolyte quantity and the anion oxidation on the cathode surface results in the decrease of LiTFSI concentration in the electrolyte.

In full-cells, the visualization of the electrolyte degradation through electrochemical performance depends on the N/P ratio. The electrochemical degradation of the electrolyte is masked in the cells with the N/P ratio close to 'one' as the extent of the anode accepting the electrons from the electrolyte oxidation is limited by its capacity. Hence, full cells are not the right choice to evaluate cells at elevated temperatures with parasitic reactions on the cathode surface. Oxidation of electrolyte over the cathode surface results in a depth-dependent cathode electrolyte interphase (CEI), with the decomposition products such as LiF and LiNSO increasing with depth. LiNSO was found in higher quantities in the RTIL with low stability and was very minimal with a stable electrolyte. Further, electrolyte oxidation directly affects the calendar aging of the cells, and it was found to vary with the extent of electrolyte stability. Overall, there are several design parameters to keep in mind before designing a cell for high-temperature operation. Full cells do not essentially portray the actual degradation taking place in the CEI.

CRediT authorship contribution statement

Sathish Rajendran: Conceptualization, Formal analysis, Writing – original draft, Writing – review & editing. **Veka Sri Ganesan:** Data curation, Formal analysis, Investigation, Writing – review & editing. **Leela Mohana Reddy Arava:** Conceptualization, Formal analysis, Funding acquisition, Investigation, Project administration, Supervision, Writing – review & editing.

Declaration of competing interest

The authors declare the following financial interests/personal relationships which may be considered as potential competing interests:

Leela Mohana Reddy Arava reports financial support was provided by National Science Foundation Division of Chemical Bioengineering Environmental and Transport Systems.

Data availability

Data will be made available on request.

Acknowledgement

This work was supported in part by the by the Advanced Energy Consortium (AEC-BEG14-02) and National Science Foundation under Grant No. 1751472. Partner companies for AEC include BHP, Exxon-Mobil, U.S. Department of Energy, Repsol, Sandia National Labs, and Total. The authors acknowledge the Lumigen Instrument Centre at Wayne State University for the HR-TEM (NSF: 2018587), EDX (NSF: MRI 0922912), NMR (NSF: 0840413) and XPS (NSF: MRI 1849578) facility.

Supplementary materials

Supplementary material associated with this article can be found, in the online version, at doi:10.1016/j.electacta.2024.144599.

References

[1] M.S. Whittingham, Lithium batteries and cathode materials, Chem. Rev. 104 (10) (2004) 4271–4302.
[2] X. Xu, W. Li, B. Xu, J. Qin, Numerical study on a water cooling system for prismatic $LiFePO_4$ batteries at abused operating conditions, Appl. Energy 250 (2019) 404–412.
[3] M.T.F. Rodrigues, G. Babu, H. Gullapalli, K. Kalaga, F.N. Sayed, K. Kato, J. Joyner, P.M. Ajayan, A materials perspective on Li-ion batteries at extreme temperatures, Nat. Energy 2 (8) (2017) 1–14.
[4] L. Bodenes, R. Naturel, H. Martinez, R. Dedryvère, M. Menetrier, L. Croguennec, J. P. Pérès, C. Tessier, F. Fischer, Lithium secondary batteries working at very high temperature: capacity fade and understanding of aging mechanisms, J. Power Sources 236 (2013) 265–275.
[5] M.J. Marczewski, B. Stanje, I. Hanzu, M. Wilkening, P. Johansson, Ionic liquids-in-salt"–a promising electrolyte concept for high-temperature lithium batteries? Phys. Chem. Chem. Phys. 16 (24) (2014) 12341–12349.
[6] H. Niu, L. Wang, P. Guan, N. Zhang, C. Yan, M. Ding, X. Guo, T. Huang, X. Hu, Recent advances in application of ionic liquids in electrolyte of lithium ion batteries, J. Energy Storage 40 (2021) 102659.
[7] M. Galiński, A. Lewandowski, I. Stępniak, Ionic liquids as electrolytes, Electrochim. Acta 51 (26) (2006) 5567–5580.
[8] N. Plylahan, M. Kerner, D.H. Lim, A. Matic, P. Johansson, Ionic liquid and hybrid ionic liquid/organic electrolytes for high temperature lithium-ion battery application, Electrochim. Acta 216 (2016) 24–34.
[9] H. Yang, G.V. Zhuang, P.N. Ross Jr, Thermal stability of LiPF6 salt and Li-ion battery electrolytes containing LiPF6, J. Power Sources 161 (1) (2006) 573–579.
[10] K. Naoi, M. Mori, Y. Naruoka, W.M. Lamanna, R. Atanasoski, The surface film formed on a lithium metal electrode in a new imide electrolyte, lithium bis (perfluoroethylsulfonylimide)[$LiN(C_2F_5SO_2)_2$], J. Electrochem. Soc. 146 (2) (1999) 462.
[11] M. Dahbi, F. Ghamouss, F. Tran-Van, D. Lemordant, M. Anouti, Comparative study of EC/DMC LiTFSI and $LiPF_6$ electrolytes for electrochemical storage, J. Power Sources 196 (22) (2011) 9743–9750.
[12] M. Dahbi, F. Ghamouss, F. Tran-Van, D. Lemordant, M. Anouti, Ester based electrolyte with lithium bis (trifluoromethane sulfonyl) imide salt for electrochemical storage devices: physicochemical and electrochemical characterization, Electrochim. Acta 86 (2012) 287–293.
[13] X. Chen, W. Xu, M.H. Engelhard, J. Zheng, Y. Zhang, F. Ding, J. Qian, J.G. Zhang, Mixed salts of LiTFSI and LiBOB for stable $LiFePO_4$-based batteries at elevated temperatures, J. Mater. Chem. A 2 (7) (2014) 2346–2352.
[14] M. Kerner, P. Johansson, Pyrrolidinium FSI and TFSI-based polymerized ionic liquids as electrolytes for high-temperature lithium-ion batteries, Batteries 4 (1) (2018) 10.
[15] S. Nagarajan, C. Weiland, S. Hwang, M. Balasubramanian, L.M.R. Arava, Depth-dependent understanding of cathode electrolyte interphase (CEI) on the layered Li-ion cathodes operated at extreme high temperature, Chem. Mater. 34 (10) (2022) 4587–4601.
[16] C.J. Jafta, X.G. Sun, H. Lyu, H. Chen, B.P. Thapaliya, W.T. Heller, M.J. Cuneo, R. T. Mayes, M.P. Paranthaman, S. Dai, Insight into the solid electrolyte interphase formation in bis (fluorosulfonyl) imide based ionic liquid electrolytes, Adv. Funct. Mater. 31 (23) (2021) 2008708.
[17] U. Pal, D. Rakov, B. Lu, B. Sayahpour, F. Chen, B. Roy, D.R. MacFarlane, M. Armand, P.C. Howlett, Y.S. Meng, Interphase control for high performance lithium metal batteries using ether aided ionic liquid electrolyte, Energy Environ. Sci. 15 (5) (2022) 1907–1919.
[18] E.I. Rogers, B. Sljukic, C. Hardacre, R.G. Compton, Electrochemistry in room-temperature ionic liquids: potential windows at mercury electrodes, J. Chem. Eng. Data 54 (7) (2009) 2049–2053.
[19] J.I. Phillips, S. Azuma, J. Lee, T. Ueda, D.S. Silvester, Cation effect on the electrochemical reduction of polyoxometalates in room temperature ionic liquids, Aust. J. Chem. 75 (11) (2022) 865–876.
[20] P. Peljo, H.H. Girault, Electrochemical potential window of battery electrolytes: the HOMO–LUMO misconception, Energy Environ. Sci. 11 (9) (2018) 2306–2309.
[21] S. Rajendran, Z. Tang, A. George, A. Cannon, C. Neumann, A. Sawas, E. Ryan, A. Turchanin, L.M.R. Arava, Inhibition of lithium dendrite formation in lithium metal batteries via regulated cation transport through ultrathin sub-nanometer porous carbon nanomembranes, Adv. Energy Mater. 11 (29) (2021) 2100666.
[22] J.C. Lassègues, J. Grondin, C. Aupetit, P. Johansson, Spectroscopic identification of the lithium ion transporting species in LiTFSI-doped ionic liquids, J. Phys. Chem. A 113 (1) (2009) 305–314.
[23] S. Menne, T. Vogl, A. Balducci, Lithium coordination in protic ionic liquids, Phys. Chem. Chem. Phys. 16 (12) (2014) 5485–5489.
[24] F. Castiglione, E. Ragg, A. Mele, G.B. Appetecchi, M. Montanino, S. Passerini, Molecular environment and enhanced diffusivity of Li^+ ions in lithium-salt-doped ionic liquid electrolytes, J. Phys. Chem. Lett. 2 (3) (2011) 153–157.
[25] I. Nicotera, C. Oliviero, W.A. Henderson, G.B. Appetecchi, S. Passerini, NMR Investigation of Ionic Liquid−LiX Mixtures: pyrrolidinium cations and $TFSI^-$ anions, J. Phys. Chem. B 109 (48) (2005) 22814–22819.
[26] F. Castiglione, M. Moreno, G. Raos, A. Famulari, A. Mele, G.B. Appetecchi, S. Passerini, Structural Organization and Transport Properties of Novel Pyrrolidinium-Based Ionic Liquids with Perfluoroalkyl Sulfonylimide Anions, J. Phys. Chem. B 113 (31) (2009) 10750–10759.
[27] A. Lewandowski, A. Świderska-Mocek, Ionic liquids as electrolytes for Li-ion batteries–an overview of electrochemical studies, J. Power Sources 194 (2) (2009) 601–609.
[28] X. Wu, K. Song, X. Zhang, N. Hu, L. Li, W. Li, L. Zhang, H. Zhang, Safety issues in lithium ion batteries: materials and cell design, Front. Energy Res. 7 (2019) 65.
[29] X. Cao, Y. Xu, L. Zhang, M.H. Engelhard, L. Zhong, X. Ren, H. Jia, B. Liu, C. Niu, B. E. Matthews, Nonflammable electrolytes for lithium ion batteries enabled by ultraconformal passivation interphases, ACS Energy Lett. 4 (10) (2019) 2529–2534.
[30] Z. Zhang, J. Yang, W. Huang, H. Wang, W. Zhou, Y. Li, Y. Li, J. Xu, W. Huang, W. Chiu, Cathode-electrolyte interphase in lithium batteries revealed by cryogenic electron microscopy, Matter 4 (1) (2021) 302–312.
[31] S. Malmgren, K. Ciosek, M. Hahlin, T. Gustafsson, M. Gorgoi, H. Rensmo, K. Edström, Comparing anode and cathode electrode/electrolyte interface composition and morphology using soft and hard X-ray photoelectron spectroscopy, Electrochim. Acta 97 (2013) 23–32.
[32] B. Zheng, J. Zhu, H. Wang, M. Feng, E. Umeshbabu, Y. Li, Q.H. Wu, Y. Yang, Stabilizing $Li_{10}SnP_2S_{12}$/Li interface via an *in situ* formed solid electrolyte interphase layer, ACS Appl. Mater. Interfaces 10 (30) (2018) 25473–25482.
[33] F. Wu, S. Fang, M. Kuenzel, A. Mullaliu, J.K. Kim, X. Gao, T. Diemant, G.T. Kim, S. Passerini, Dual-anion ionic liquid electrolyte enables stable Ni-rich cathodes in lithium-metal batteries, Joule 5 (8) (2021) 2177–2194.
[34] F. Li, J. He, J. Liu, M. Wu, Y. Hou, H. Wang, S. Qi, Q. Liu, J. Hu, J. Ma, Gradient solid electrolyte interphase and lithium-ion solvation regulated by bisfluoroacetamide for stable lithium metal batteries, Angew. Chem. Int. Ed. 60 (12) (2021) 6600–6608.
[35] G. Chen, J. Zhang, S. Yang, Fabrication of hydrophobic fluorinated amorphous carbon thin films by an electrochemical route, Electrochem. Commun. 10 (1) (2008) 7–11.
[36] F. Wu, G.T. Kim, T. Diemant, M. Kuenzel, A.R. Schür, X. Gao, B. Qin, D. Alwast, Z. Jusys, R.J. Behm, Reducing capacity and voltage decay of Co-free $Li_{1.2}Ni_{0.2}Mn_{0.6}O_2$ as positive electrode material for lithium batteries employing an ionic liquid-based electrolyte, Adv. Energy Mater. 10 (34) (2020) 2001830.
[37] J.D. McBrayer, M.T.F. Rodrigues, M.C. Schulze, D.P. Abraham, C.A. Apblett, I. Bloom, G.M. Carroll, A.M. Colclasure, C. Fang, K.L. Harrison, Calendar aging of silicon-containing batteries, Nat. Energy 6 (9) (2021) 866–872.